THE JOURNAL OF PHYSICAL CHEMISTRY B

ARTICLE

pubs.acs.org/JPCB

Pressure-Induced Phase Transitions in Ammonium Squarate: A Supramolecular Structure Based on Hydrogen-Bonding and π-Stacking Interactions

Shourui Li, Kai Wang, Mi Zhou, Qian Li, Bingbing Liu, Guangtian Zou, and Bo Zou*

State Key Laboratory of Superhard Materials, Jilin University, Changchun 130012, China

Supporting Information

ABSTRACT:

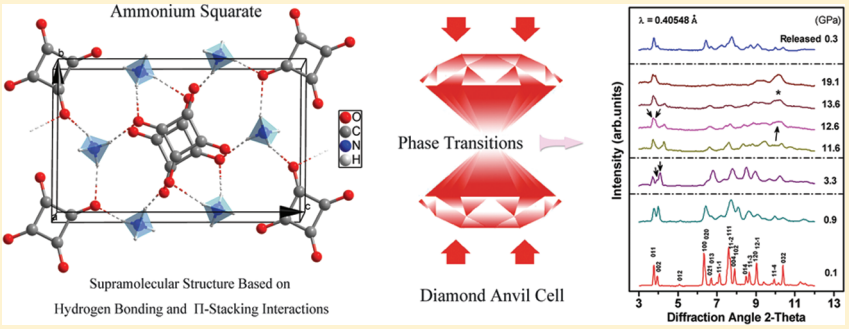

We report the results of high-pressure Raman and X-ray diffraction measurements performed on ammonium squarate ($(NH_4)_2C_4O_4$, AS), a representative supramolecular architecture based on hydrogen bonding and π-stacking interactions, at various pressures up to 19 GPa. Two phase transitions at ~2.7 GPa and in the pressure range of 11.1−13.6 GPa were observed. Both Raman and XRD results provide convincing evidence for these two phase transitions. The first phase transition is attributed to the rearrangements of hydrogen-bonding networks, resulting in the symmetry transformation from $P2_1/c$ to $P1$. The second one, which is identified as an order−disorder phase transition, arises from significant modifications of squarate rings and random orientations of NH_4^+ cations. The cooperative effects between hydrogen-bonding and π-stacking interactions, as well as mechanisms for the phase transitions, are discussed by virtue of the local structure of AS.

INTRODUCTION

Supramolecular chemistry has attracted considerable attention since the concept was proposed.[1,2] It is an interdisciplinary subject that concerns the synthesis, properties, and applications of "various molecular assemblies".[3−5] Recently, there has been much work on designing building blocks with desired properties.[6,7] It is noncovalent interactions that hold the blocks together as a whole. Apparently, how architectures form via cooperative effects of noncovalent interactions is the basic issue in supramolecular chemistry. The supramolecular interactions, including hydrogen bonding and π-stacking, play a critical role in crystal engineering. Investigations of noncovalent interactions can provide a better understanding of the nature and cooperative mechanisms of these interactions in supramolecular architectures, as well as a clue for designing supramolecular devices with specific functions. Especially, hydrogen bonding which combines directionality with strength, [8] π-stacking, and their cooperativity have been extensively exploited in crystal engineering.[9−12] Moreover, pressure on a tens of gigapascals scale can cause significant variations in relatively weak interactions and be utilized as a powerful tool to uncover phenomena hidden at ambient pressure.[13−16] Hence, high-pressure studies of noncovalent interactions and their cooperativity in the stability of supramolecular architectures are of fundamental and practical importance.

To our knowledge, there have been scarce explorations concerning cooperativity of various weak interactions under high-pressure conditions, even if much endeavor has been done for investigations on individual interactions.[17,18] It is well-known that pressure and temperature are the fundamental thermodynamic parameters which are widely used to develop a comprehensive understanding of material laws. According to the equation of Gibbs free energy, which determines phase stability at various $P-T$ conditions, pressure can be more effective in inducing phase changes because of its broad range. Meanwhile, pressure allows precise modification of the intermolecular distance, which controls noncovalent interactions that determine the properties of supramolecular materials. Such pressure-tuning investigations can provide valuable information for understanding cooperative mechanisms in new structures and existing ones,

Received: March 31, 2011
Revised: June 23, 2011
Published: June 24, 2011

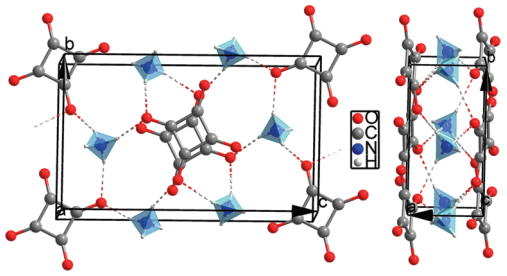

Figure 1. Crystal structure of AS under ambient conditions. The hydrogen bonds are marked as dashed lines. The tetrahedron represents the ammonium cation with the nitrogen atom in the center and hydrogen atoms at the four vertices.

as well as guidance for searching and designing new supramolecular systems with targeted functions. That is the principal driving force for our systematic investigations in a series of supramolecular materials with various noncovalent interactions in them. Recently, several works concerning the cooperativity within supramolecular crystals under high pressure have been published. The melamine−boric acid adduct (M·2B) undergoes a reversible pressure-induced amorphization (PIA) at 18 GPa.[19] The cyanuric acid−melamine adduct (CA·M) experiences an irreversible phase transition around 4 GPa.[20] Regarding guanidinium nitrate (GN), a phase transition at 1 GPa is also evidenced at the expense of collapse of 2-D hydrogen-bonding networks.[21,22] Halogen bonding has proven to be an effective noncovalent interaction to stabilize the structure of cyanuric chloride up to 30 GPa.[23] All the results suggest that noncovalent interactions can alter or even govern behaviors of a supramolecular system under high pressure. Besides, the adduct formed between squaric acid and 4,4′-bipyridine goes through two pressure-induced phase transitions at 1.8 and 2.6 GPa, and the proton-transfer nature is expected to play a vital role in the transitions.[24]

As part of our systematic high-pressure studies on supramolecular systems, ammonium squarate ($(NH_4)_2C_4O_4$, AS) is chosen. Under ambient conditions, it crystallizes in the monoclinic space group $P2_1/c$ (a = 3.7054(3) Å, b = 7.2573(5) Å, c = 11.9315(8) Å, β = 97.928(4)°) with Z = 2,[25] as shown in Figure 1. It is worth noting that AS presents a unique double-layered structure. The squarate ions displayed in the (001) plane and NH_4^+ cations are intercalated between squarate anion layers via N−H···O hydrogen bonds. The squarate anions in the same plane display two different line arrangements with about 30° rotation, while the squarate anions of adjacent planes do not present any rotation. The π-stacking interaction exists between squarate rings as a result of electron delocalization. Therefore, it is hydrogen-bonding and π-stacking interactions that modulate each other and are responsible for the crystal packing.[25] It is reported that an ammonium amide ionic crystal consisting of alternate layers of NH_4^+ and NH_2^- ions is formed with ammonia as the raw material at 90 GPa, and the ionic crystal is predicted to be stable over a wide pressure range.[26] Moreover, squaric acid has been a research topic for several decades due to its special structure and properties.[27] It is suggested that squaric acid can provide guidance for the design of genuine organic ferroelectrics owing to its 4-fold symmetric permanent dipoles induced by the tautomerism.[28] The squarate ion, in its turn, is a very versatile synthon in building up supramolecular architectures where hydrogen bonding plays a decisive role.[24,29,30] Therefore, it is of significant interest to study the behaviors of AS under high pressure, and special attention is paid to if and how the two noncovalent interactions dominate the new high-pressure phases. Meanwhile, AS can be used as a model for studies of more complex supramolecular systems, including biochemical materials and proteins, where hydrogen-bonding and π-stacking interactions are commom.[31] Furthermore, four life elements (C, H, N, and O) consitute AS, and the knowledge of its high-pressure behaviors is expected to be a great help for various biogeochemical processes.[32]

In this work, in situ Raman spectroscopy and synchrotron X-ray diffraction (XRD) combined with symmetric diamond anvil cell (DAC) techniques have been conducted to study the stability of AS at high pressure. Raman spectroscopy has been used to monitor phase changes of the title supramolecular crystal. Special attention is paid to the modes related to π-stacking and hydrogen-bonding interactions. Particularly, high-pressure angle-dispersive synchrotron X-ray diffraction (ADXRD) can give valuable information on molecular orientations and conformations in new high-pressure phases and helps in the comprehensive understanding of how noncovalent interactions dominate new structures. The primary goal of this work is to offer a better understanding for the nature of the two noncovalent interactions and the stability of the title supramolecular architecture under high pressure. The analysis of the structural changes, as well as cooperative effects between hydrogen-bonding and π-stacking interactions, has been performed.

EXPERIMENTAL SECTION

AS was prepared via the conventional slow evaporation method in terms of the procedures reported elsewhere.[25] The sample was recrystallized in deionized water two times before being used for high-pressure experiments, and the purity was confirmed by both Raman and XRD results. On the basis of the uniformity of Raman profiles between the observed pattern and the published one, we follow their assignments.[25] The symmetric DAC furnished with 0.4 mm diamond cells was used to perform all the high-pressure measurements. The powdered sample with a grain size of less than a few micrometers and two or three ruby chips were loaded into the hole, which had been drilled to 130 μm diameter in the preindented T301 steel gasket and served as the sample compartment. The well-established ruby luminescence technique was employed to do the pressure calibration. The pressure conditions were detected by monitoring the separation between R1 and R2 lines.[33] All experiments were performed at room temperature.

Raman spectra were measured with the Renishaw inVia Raman microscope using the backscattering configuration. The 514.5 nm line of an argon ion laser was used as the excitation source. The standard silicon line was applied to calibrate the Raman system before each experiment. The laser beam passed through a vertical polarizer and a tunable filter and was focused onto the sample using a Nikon 50× microscope objective with high numerical aperture. The spectral resolution was approximately 1 cm^{-1}. The output power of the laser was set to 10 mW to avoid sample heating. Each new acquisition was carried out several minutes later after elevation of the pressure, aiming to restrain any kinetic factor during the measurements. Although no transmitting medium was applied as the usual ones could overlap the NH stretching region, quasi-hydrostatic conditions were obtained due to the softness of AS, which was common among

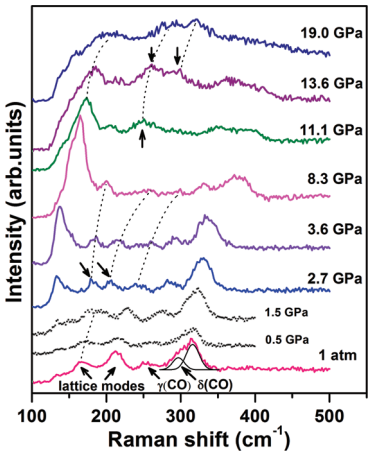

Figure 2. Representive Raman spectra of AS between 100 and 500 cm^{-1} at various pressures. The dotted lines are illustrated for the sake of clarity of the lattice modes' evolution.

organic materials.[34] Meanwhile, the high-pressure Raman scattering and synchrotron XRD experiments under hydrostatic pressure using the 16:3:1 mixture of methanol−ethanol−water as a pressure-transmitting medium (PTM) were conducted. The results under hydrostatic pressure conditions are the same in essence as the results without any PTM, implying the acceptability of the quality of the pressure conditions (Figures S1 and S2, Supporting Information). The Raman profiles were fit with a combination of Gaussian and Lorentzian functions.

The ADXRD measurements were conducted without any PTM at the High Pressure Collaborative Access Team's (HPCAT's) 16 BMD beamline facility of the Advanced Photon Source (APS) at Argonne National Laboratory. The 0.40548 Å beam with a diameter of 10 μm was utilized for pattern collection. The second run of ADXRD experiments was done on the 4W2 beamline at the High Pressure Station of the Beijing Synchrotron Radiation Facility (BSRF). The mixture of methanol−ethanol−water (16:3:1) was used as the PTM. The monochromatic 0.6199 Å radiation with a 30 × 30 spot was used for data collection. The typical acquisition time was set to 300 s for both measurements owing to light elements (C, H, N, O) in AS. The image-plate area detector (Mar345) was adopted to collect diffraction data. Then the collected 2-D images were first integrated and analyzed using the FIT2D program to gain plots of intensity versus 2θ.[35] The obtained patterns were analyzed with the commercial Materials Studio 5.0 program to determine the precise lattice parameters and candidate space groups.

Ab initio calculations were performed with the pseudopotential plane-wave methods based on density functional theory implemented in the CASTEP package. The local density approximation exchange-correlation functional was applied during the calculations. Vanderbilt-type ultrasoft pseudopotentials were employed with a plane-wave cutoff energy of 750 eV.

RESULTS AND DISCUSSION

The evolution of Raman spectra ranging from 100 to 500 cm^{-1} is shown in Figure 2. Two lattice modes at 168.8 and 212.6 cm^{-1} are observed at ambient conditions. The two new lattice modes marked by arrows in the curve of 2.7 GPa are observed, indicating the transition from phase I to phase II. The splitting of lattice modes accounts for the lower symmetry in phase II combined with other experimental data that will be discussed later.[36,37] With further compression above 2.7 GPa, the lattice modes exhibit normal blue shifts, shown in Figure 4. In the plot of 8.3 GPa in Figure 1, the two lattice modes in the 210−310 cm^{-1} region become so weak as to be on the margin of what can be traced. At 11.1 GPa, the two modes lose their intensities absolutely with the emergence of a new lattice mode at 249 cm^{-1} marked by an arrow, implying the beginning of the phase transition from phase II to phase III. Another lattice mode appears marked by an arrow with further compression to 13.6 GPa, indicating accomplishment of this transition. The three lattice modes in phase III keep their initial distribution in position and intensity without any discontinuous change up to 19.0 GPa, the highest pressure of the experiment. There are also three internal vibrations in this region, with two of them assigned as γ(CO) and δ(CO), as shown in Figure 1. Below 11.1 GPa, the internal modes exhibit normal blue shifts without abrupt variations except that the doublet bands cannot be resolved anymore at 2.7 GPa. There is dramatic weakness in the intensities of the internal vibrations at 11.1 GPa. With further compression above 11.1 GPa, the internal vibrations lose their intensities gradually and vanish into the scattering background eventually. The variations of the internal vibrations reveal that squarate ions undergo significant modifications across the second transition as a result of the expected enhancement of π-stacking interaction between adjacent squarate ions.

The evolution of Raman spectra from 600 to 1300 cm^{-1} as a function of pressure is depicted in Figure 3a. The ring bending mode with B_{2g} symmetry and the ring breathing mode with A_{1g} symmetry show normal blue shifts up to 2.7 GPa. In the phase II zone, the ring bending mode evolves into the doublet bands at 3.6 GPa and the triplet bands at 8.3 GPa, shown in Figure 3a. Similarly, the ring breathing mode appears asymmetric and splits into a doublet at 2.7 GPa. Another weaker band emerges marked by an arrow at 9.6 GPa. The splitting of the ring vibrations indicates that the symmetry of the squarate ion decreases progressively with increasing pressure. This is primarily due to the expected enhancement of π-stacking interaction between neighboring layers.[38] Over the 11.1−13.6 GPa range, the bands change gradually and finally evolve into a stable pattern at 13.6 GPa, with two weak bands vanishing, as shown in Figure 3a, and the pattern remains unchanged all the way up to 19.0 GPa. For the ν(CC) mode, there is no abrupt change until 4.7 GPa, where the band starts to split into two. The observed doublet bands remain undisturbed up to 19.0 GPa. The band marked by an asterisk arises from the influence of the fluorescent lamp.

Figure 3b summarizes the evolution of the Raman spectra of AS in the 1350−1980 cm^{-1} region. The two NH bending modes merge into a broad band at 1.5 GPa and cannot be detected anymore above 11.1 GPa. Apart from the influence of the background scattering, the disappearance of the NH vibration is principally due to random arrangements of NH_4^+ cations or proton disorder. The two bands located at 1577 and 1611 cm^{-1}, which are considered as a combination of ν(CC) and ν(CO), change continuously with ascending pressure up to 11.1 GPa. There is a triplet splitting of one band at this critical point, implying the transition from phase II to phase III. The bands become broader with increasing pressure and cannot be resolved beyond 17.1 GPa. As shown in Figure 3b, the mode corresponding to ν(CO) tends to split into two owing to its broad and asymmetric feature, and the two bands are well-resolved below 10.9 GPa. The band of higher frequency displays progressive loss of intensity and vanishes completely over the 11.1−13.6 GPa

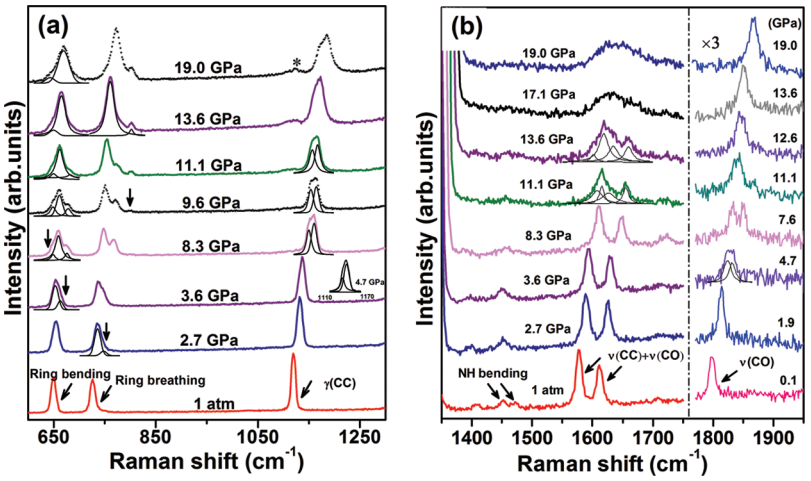

Figure 3. Selected Raman spectra of AS at various pressures in the ranges of (a) 600−1300 cm^{-1} and (b) 1350−1950 cm^{-1}. The peak marked by an asterisk in (a) originates from the influence of the fluorescent lamp.

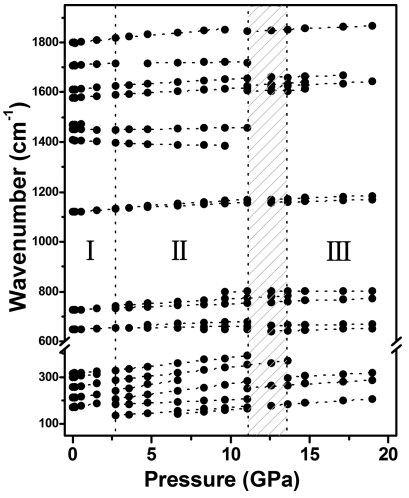

Figure 4. Pressure dependence of Raman peak positions of internal modes and external modes in the range of 100−1950 cm^{-1}. Linear fits are performed for clarity. The dotted line and shadow region represent boundaries of different phases.

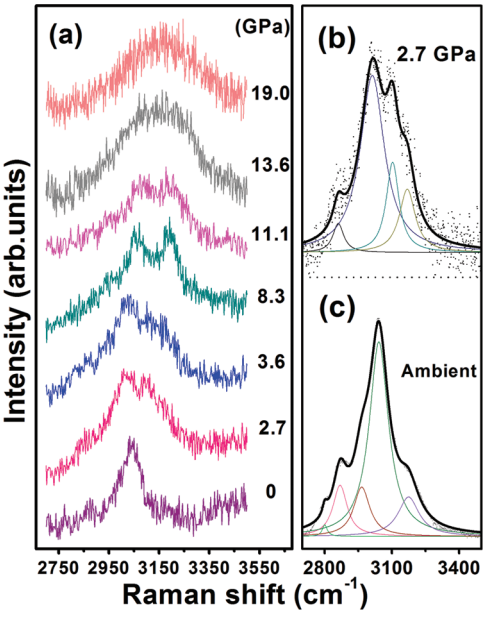

Figure 5. (a) Evolution of Raman spectra of AS in the NH stretching region at selected pressures. (c) and (b) illustrate the decomposition of the NH stretching modes at ambient conditions and 2.7 GPa, respectively.

region, indicative of the second phase transition. Another band remains stable in the phase III zone. The observed results combined with the changes of the ring modes lead to the conclusion that the symmetry of $C_4O_4^{2-}$ anions becomes lower with increasing pressure up to 11.1 GPa. Then the anions undergo significant modifications during the second phase transition.

The frequency shifts of the external and internal modes ranging from 100 to 1950 cm^{-1} are illustrated in Figure 4. It is obvious that AS undergoes two phase transitions at 2.7 GPa and in the 11.1−13.6 GPa range from the evolution of the lattice modes. The behaviors of the modes corresponding to ring vibrations appear to be complex because of enhanced π-stacking interaction. Note that the squarate anion reveals a high degree of electronic delocalization as the CC and CO bond distances are nearly identical at ambient conditions. Raman spectra ranging from 1000 to 1200 cm^{-1} representing CC stretching have enabled identification of the extent of the delocalization.[25] Then the question of whether the electronic localization effect is involved in the band splitting arises. To address this question, we reexamine the Raman spectra of several squarate salts and squaric acid itself with different degrees of electronic delocalization. The transition-metal compounds (Fe^{2+}, Co^{2+}, Ni^{2+}, Cu^{2+}, Zn^{2+}) with a high degree of electronic delocalization reveal only one band in this range similar to AS,[39] whereas the substances squaric acid and rubidium hydrogen squarate with a low degree of delocalization exhibit two well-separated bands with more than 100 cm^{-1} as the interval,[40,41] rather than the doublet bands. Thus, we attribute the band splitting to symmetry lowering of the squarate ions.

Figure 5 depicts Raman spectra in the NH stretching region at selected pressures. As shown in Figure 5c, the spectrum in this range is comprised of five bands at ambient conditions. However,

dx.doi.org/10.1021/jp202975q |J. Phys. Chem. B 2011, 115, 8981–8988

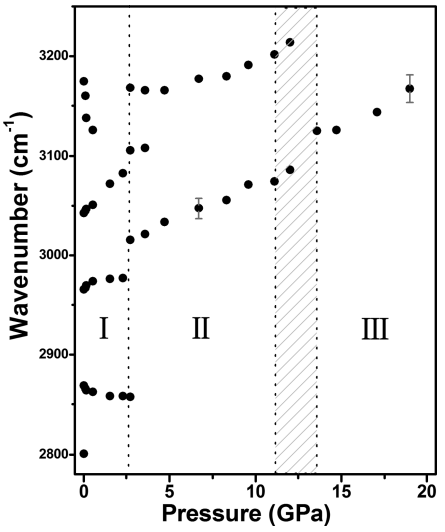

Figure 6. Pressure dependence of the peak positions in the NH stretching region. The dotted line and the shadow area stand for boundaries of different phases. Representative error bars are shown to display errors of the experimental data.

only four bands can be resolved once the sample is loaded into the DAC. It is obvious that NH stretching modes undergo a redistribution of intensities and positions at 2.7 GPa, with the details illustrated in Figure 5b. In other words, there are rearrangements of hydrogen bonds across the first transition.[21,22,32] With further increasing pressure, the band of high frequency gains intensity gradually accompanied by another band vanishing. The remaining two bands become broad suddenly at 11.1 GPa and no longer discernible at 13.6 GPa, suggesting the second phase transition, shown in Figure 5a. The broad characteristic of NH stretching suggests that the orientations of ammonium cations are random, consistent with disappearance of NH bending in the phase III range. The proton disorder has been observed in many substances at high pressure.[34,42,43] The pressure dependence of the peak positions is shown in Figure 6. Apparently, the peak positions change dramatically at 2.7 GPa, indicating the first phase transition. Below 2.7 GPa, the two modes (2868 and 3175 cm^{-1}) exhibit red shifts while another two (2965 and 3041 cm^{-1}) show blue shifts with increasing pressure at different rates. This can be understood in terms of various hydrogen bonds with different strengths and parameters.[44,45] The typical hydrogen bond can be denoted as D−H···A, where D and A mean donor and acceptor, respectively. For weak and moderate hydrogen bonds, pressure can shorten the D−A distance followed by contraction of the H···A distance owing to the increasing electrostatic attraction between H and A. Then the D−H distance is extended, resulting in a red shift of the D−H stretching modes, while the blue shift can be traced for strong hydrogen bonds because of sustaining enhancement of hydrogen bonds at high pressure. Furthermore, the rate of the blue shift regarding the mode at 2965 cm^{-1} becomes lower with increasing pressure, which suggests it is hard to compress the hydrogen bond at higher pressure over 0−2.7 GPa. Meanwhile, the rate of the red shift regarding the mode at 2868 cm^{-1} becomes lower, implying that the hydrogen bond gains its strength on compression.

To demonstrate the existence of phase transitions of AS under pressure conditions, we performed the ADXRD experiment, which is believed to offer straightforward evidence for phase

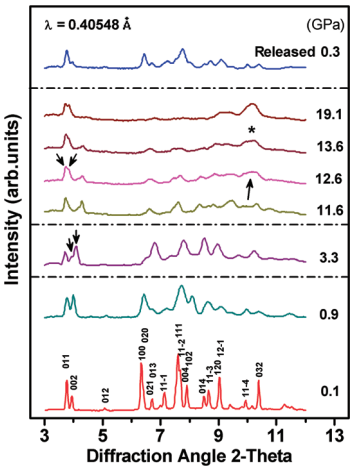

Figure 7. Representative XRD patterns of AS at high pressures. The wavelength for data collection is 0.40548 Å. An asterisk marks the amorphous yet characteristics peak in the curve of 13.6 GPa. The top pattern is the one collected when pressure was released to 0.3 GPa.

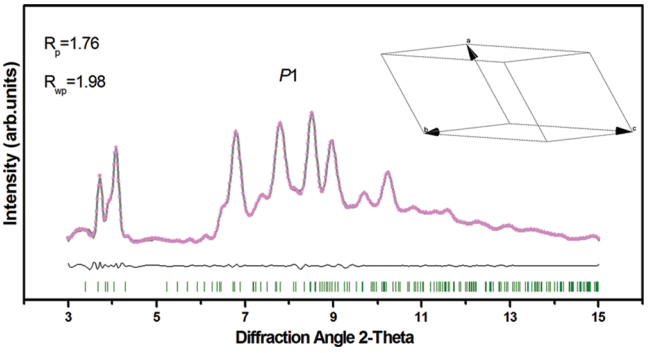

Figure 8. Pawley refinement of the pattern collected at 3.3 GPa. The obtained space group *P*1 is depicted as the inset. The gray line represents the fit residual beneath.

transitions. The evolution of the XRD patterns is illustrated in Figure 7. As can be seen, the quality of the data is not flawless. For example, some peaks become broad and weak as well as merge together even at the relatively low pressure of 0.9 GPa. This restrains any accurate Rietveld refinement to acquire atomic positions in the unit cell.[32,46] However, the results can still provide evidence for phase transitions. At 3.3 GPa, the diffraction profile changes significantly, indicating the first phase transition. The pattern at 3.3 GPa is best described with triclinic *P*1 symmetry, and the indexed parameters are a = 6.65(7) Å, b = 8.03(6) Å, c = 9.13(7) Å, α = 131.55(7)°, β = 120.49(9) °, γ = 68.77(2)°, and V = 314.91(1) $Å^3$, as shown in Figure 8. Over the 11.6−13.6 GPa range, AS undergoes the second phase transition, as demonstrated by peak splitting and emergence of new peaks. Meanwhile, a broad but relatively intense peak marked by an asterisk emerges at 13.6 GPa, which persists up to 19.1 GPa. The diffuse peak in phase III is consistent with random orientations of ammonium ions deduced from the evolution of the NH bending and stretching modes. In light of the weak intensities as well as the broad and amorphous peak in phase III, we do not provide any intensity refinements to obtain the information about symmetry. However, we propose that squarate cations are likely still in the ordered state since the peaks with low diffraction

dx.doi.org/10.1021/jp202975q |*J. Phys. Chem. B* 2011, 115, 8981–8988

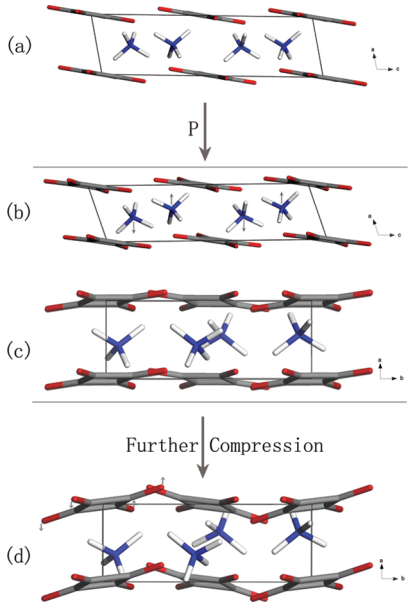

Figure 9. (a) Double-layered structure of AS at ambient pressure. (b, c) Double-layered structure of AS at moderate pressure. (d) Double-layered structure of AS at high pressure.

angles are relatively sharp, shown in the plot of 19.1 GPa in Figure 7. Additionally, the released pattern demonstrates that AS returns to its initial state compared with the data at 0.3 GPa.

To understand what changes of the local structure of AS occur on earth at high pressure, we performed ab initio calculations using the pseudopotential plane-wave methods based on density functional theory. According to the calculated results (shown in Figure 9), NH_4^+ cations move to new positions with compression (indicated by arrows in Figure 9b) and $C_4O_4^{2-}$ anions tilt slightly from the average sheet, yet each anion retains the planar structure. The results are in excellent agreement with the evolution of the N−H stretching region and confirm rearrangements of hydrogen bonds across the first phase transition. With further compression, $C_4O_4^{2-}$ anions display significant deformations, with the oxygen atoms deviating from the anion plane, and the plane of the squarate ion evolves into a wave-shaped structure (Figure 9d). The calculated results can contribute to the understanding of π-stacking and hydrogen-bonding interactions.

Here, we talk about how π-stacking and hydrogen-bonding interactions dominate the stability of AS under high pressure qualitatively, combined with the calculated structural models. Below 2.7 GPa, the NH stretching modes show a red or blue shift due to various strengths. The ring-related modes, including ring bending and ring breathing, CC vibration modes, and CO vibration modes all reveal blue shifts without abrupt changes. Meanwhile, the increasing pressure causes adjacent squarate and ammonium ions to become closer inevitably, which leads to strengthening of the electrostatic interaction and an increase in the total Gibbs free energy correspondingly.[47] At 2.7 GPa, rearrangements of the hydrogen-bonding networks occur to cause AS to adopt new orientations, resulting in the first phase transition. Nevertheless, the squarate ions remain relatively undisturbed as the ring-related vibrations exhibit no dramatic changes with the exception of the asymmetry of ring breathing at this critical point. However, the ring breathing mode involves atomic motions only in the squarate anion plane perpendicular to the direction of π-stacking interactions. Therefore, π-stacking interactions play a minor role compared with hydrogen bonds, although the spacing between adjacent planes is expected to decrease with increasing pressure. This cooperative relationship between these two noncovalent interactions can be explained by taking into account the unique structure of AS. On one hand, the π-stacking interaction between neighboring squarate ions is the representative face-to-face type where $\pi-\pi$ repulsion dominates.[25,38] The interplanar distance of squarate ions in AS is relatively large (3.41 Å) compared with those of sodium and potassium salts (3.14 and 3.27 Å, respectively).[25] Therefore, the repulsive interaction gains its strength rather slowly with ascending pressure at the beginning because the repulsive interaction is inversely proportional to the separation of the two negatively charged π-electron clouds.[38] On the other hand, the ammonium cations are located in the channels formed by the squarate anions, shown in Figure 1. Consequently, the squarate anions are less influenced although the hydrogen bonds have rearranged at 2.7 GPa. With further compression to about 11.1 GPa, the hydrogen bonds continue to be strengthened, evidenced by overall blue shifts of the NH stretching modes, while modes related to the ring exhibit complex behaviors owing to enhancement of the π-stacking interaction. As the adjacent two squarate ions get closer, the repulsive interaction is rapidly increased,[48] which must be compensated for by attracting interactions with farther ions.[47] Therefore, squarate ions are driven to undergo deformations gradually, which is confirmed by the increasing number of ring bending and ring breathing modes. When the pressure is in the range of 11.1−13.6 GPa, π-stacking and hydrogen-bonding interactions cannot afford the increased free energy anymore, and then AS adopts another new conformation to reduce the free energy. Concurrently, the squarate ions undergo significant modifications, as evidenced from the evolution of ring bending and breathing in Figure 3a, and the hydrogen bonds evolve into a distorted state, as demonstrated by the vanishing of the NH bending peaks and an amorphous peak corresponding to NH stretching.[34] In other words, ammonium ions adopt random orientations above 13.6 GPa. This cooperative effect can also be interpreted by the nature of the local structure. Because squarate rings experience dramatic modifications across the second phase transition, the oxygen atoms are forced into new balanced positions accordingly via covalent bonds. However, hydrogen bonds with oxygen atoms as acceptors do not have sufficient strength to rotate the ammonium cations.[34] Consequently, ammonium cations adopt random orientations as a result of competition between hydrogen bonds and close packing. Above 13.6 GPa, π-stacking and hydrogen-bonding interactions dominate new conformations synergetically up to 19.0 GPa.

The cooperative relationships between π-stacking and hydrogen-bonding interactions under high pressure are measured and supported by Raman spectra. The evolution of lattice modes reveals two phase transitions over 0−19.0 GPa, which is also confirmed by XRD results. The Pawley refinements manifest that phase II has much lower $P1$ symmetry compared with the ambient phase, which is consistent with the splitting of the lattice mode. In addition, synchrotron XRD results suggest phase III has the amorphous characteristic because of the occurrence of a broad peak, which is consistent with random orientations of ammonium ions. Finally, we point out that further high-pressure single-crystal X-ray diffraction and neutron diffraction investigations are required to gain precise information on atomic

positions, including hydrogen atoms, which are expected to provide crucial information about cooperative relationships between these two noncovalent interactions.

CONCLUSION

We have studied phase transitions of AS under high pressure by virtue of monitoring the evolutions of Raman spectra and synchrotron XRD patterns. AS adopts a new conformation at 2.7 GPa arising from rearrangements of hydrogen-bonding networks. However, the π-stacking interaction manifests itself a much less important factor in comparison with hydrogen bonds. The squarate rings go through a series of modifications because π-stacking is enhanced over the range of 2.7−11.1 GPa. With further compression, AS takes another new conformation accompanied by significant modifications of squarate anions and random arrangements of ammonium cations. We attribute these cooperative relationships to the nature of the local structure of AS. Investigations on cooperative effects of various noncovalent interactions under high pressure can be of irreplaceable use to crystal engineering and comprehensive understanding of the nature of structure−property relationships.

ASSOCIATED CONTENT

Supporting Information. Selected Raman spectra and representative XRD patterns of AS. This material is available free of charge via the Internet at http://pubs.acs.org.

AUTHOR INFORMATION

Corresponding Author
*E-mail: zoubo@jlu.edu.cn.

ACKNOWLEDGMENT

We are grateful to Dr. Ho-kwang Mao for help with the experiments. This work was supported by the National Natural Science Foundation of China (Grants 21073071, 20773043, and 51025206) and the National Basic Research Program of China (Grants 2011CB808200 and 2007CB808000). This work was performed at the HPCAT's 16 BMD beamline facility of the APS at Argonne National Laboratory. The HPCAT is supported by the Carnegie Institution of Washington, the Carnegie/DOE Alliance Center, the University of Nevada, Las Vegas, and Lawrence Livermore National Laboratory through funding from the Department of Energy (DOE) National Nuclear Security Administration, DOE Basic Energy Sciences (BES), and National Science Foundation. APS is supported by DOE-BES (Grant DE-AC02-06CH11357). Portions of this work were performed at the 4W2 HP-Station, BSRF, which is supported by the Chinese Academy of Sciences (Grants KJCX2-SW-N20 and KJCX2-SW-N03).

REFERENCES

(1) Lehn, J. M. *Science* **1985**, *227*, 849.
(2) Lawrence, D. S.; Jiang, T.; Levett, M. *Chem. Rev.* **1995**, *95*, 2229.
(3) Wathier, M.; Grinstaff, M. W. *J. Am. Chem. Soc.* **2008**, *130*, 9648.
(4) Davis, J. T.; Spada, G. P. *Chem. Soc. Rev.* **2007**, *36*, 296.
(5) Ciesielski, A.; Schaeffer, G.; Petitjean, A.; Lehn, J. M.; Samori, P. *Angew. Chem., Int. Ed.* **2009**, *121*, 2073.
(6) Cordier, P.; Tournilhac, F.; Soulié-Ziakovic, C.; Leibler, L. *Nature* **2008**, *451*, 977.
(7) Perry, J. J., IV; Perman, J. A.; Zaworotko, M. J. *Chem. Soc. Rev.* **2009**, *38*, 1400.
(8) Braga, D.; Grepioni, F. *Acc. Chem. Res.* **2000**, *33*, 601.
(9) Ajayaghosh, A.; George, S. J. *J. Am. Chem. Soc.* **2001**, *123*, 5148.
(10) Roesky, H. W.; Andruh, M. *Coord. Chem. Rev.* **2003**, *236*, 91.
(11) Du, M.; Cai, H.; Zhao, X. J. *Inorg. Chim. Acta* **2006**, *359*, 673.
(12) Song, B.; Wei, H.; Wang, Z. Q.; Zhang, X.; Smet, M.; Dehaen, W. *Adv. Mater.* **2007**, *19*, 416.
(13) Allan, D. R.; Blake, A. J.; Huang, D. G.; Prior, T. J.; Schröder, M. *Chem. Commun.* **2006**, *39*, 4081.
(14) Boldyreva, E. V. *Acta Crystallogr., A* **2008**, *64*, 218.
(15) Orgzall, I.; Emmerling, F.; Schulz, B.; Franco, O. *J. Phys.: Condens. Matter* **2008**, *20*, 295206.
(16) Murli, C.; Song, Y. *J. Phys. Chem. B* **2010**, *114*, 9744.
(17) Chang, H. C.; Jiang, J. C.; Su, C. C.; Lu, L. C.; Hsiao, C. J.; Chuang, C. W.; Lin, S. H. *J. Phys. Chem. A* **2004**, *108*, 11001.
(18) Okuchi, T.; Cody, G. D.; Mao, H. K.; Hemley, R. J. *J. Chem. Phys.* **2005**, *122*, 244509.
(19) Wang, K.; Duan, D. F.; Wang, R.; Lin, A. L.; Cui, Q. L.; Liu, B. B.; Cui, T.; Zou, B.; Zhang, X.; Hu, J. Z.; Zou, G. T.; Mao, H. K. *Langmuir* **2009**, *25*, 4787.
(20) Wang, K.; Duan, D. F.; Wang, R.; Liu, D.; Tang, L. Y.; Cui, T.; Liu, B. B.; Cui, Q. L.; Liu, J.; Zou, B.; Zou, G. T. *J. Phys. Chem. B* **2009**, *113*, 14719.
(21) Wang, R.; Li, S. R.; Wang, K.; Duan, D. F.; Tang, L. Y.; Cui, T.; Liu, B. B.; Cui, Q. L.; Liu, J.; Zou, B.; Zou, G. T. *J. Phys. Chem. B* **2010**, *114*, 6765.
(22) Katrusiak, A.; Szafrański, M.; Podsiadlo, M. *Chem. Commun.* **2011**, *47*, 2107.
(23) Wang, K.; Duan, D. F.; Zhou, M.; Li, S. R.; Cui, T.; Liu, B. B.; Liu, J.; Zou, B.; Zou, G. T. *J. Phys. Chem. B* **2011**, *115*, 4639.
(24) Martins, D. M. S.; Middlemiss, D. S.; Pulham, C. R.; Wilson, C. C.; Weller, M. T.; Henry, P. F.; Shankland, N.; Shankland, K.; Marshall, W. G.; Ibberson, R. M.; Knight, K.; Moggach, S.; Brunelli, M.; Morrison, C. A. *J. Am. Chem. Soc.* **2009**, *131*, 3884.
(25) Georgopoulos, S. L.; Diniz, R.; Rodrigues, B. L.; Yoshida, M. I.; de Oliveira, L. F. C. *J. Mol. Struct.* **2005**, *753*, 147.
(26) Pickard, C. J.; Needs, R. J. *Nat. Mater.* **2008**, *7*, 775.
(27) Moritomo, Y.; Koshihara, S.; Tokura, Y. *J. Chem. Phys.* **1990**, *93*, 5429.
(28) Horiuchi, S.; Tokunaga, Y.; Giovannetti, G.; Picozzi, S.; Itoh, H.; Shimano, R.; Kumai, R.; Tokura, Y. *Nature* **2010**, *463*, 789.
(29) Braga, D.; Grepioni, F. *Chem. Commun.* **1998**, *8*, 911.
(30) Fisher, M. G.; Gale, P. A.; Light, M. E.; Quesada, R. *CrystEngComm* **2008**, *10*, 1180.
(31) Schall, O. F.; Gokel, G. W. *J. Org. Chem.* **1996**, *61*, 1449.
(32) Mishra, A. K.; Murli, C.; Garg, N.; Chitra, R.; Sharma, S. M. *J. Phys. Chem. B* **2010**, *114*, 17084.
(33) Mao, H. K.; Bell, P. M.; Shaner, J. W.; Steinberg, D. J. *J. Appl. Phys.* **1978**, *49*, 3276.
(34) Rao, R.; Sakuntala, T.; Arora, A. K.; Deb, S. K. *J. Chem. Phys.* **2004**, *121*, 7320.
(35) Hammersley, A. P.; Svensson, S. O.; Hanfland, M.; Fitch, A. N.; Hausermann, D. *High Pressure Res.* **1996**, *14*, 235.
(36) Banerji, A.; Deb, S. K. *J. Phys. Chem. B* **2007**, *111*, 10915.
(37) Lamelas, F. J.; Dreger, Z. A.; Gupta, Y. M. *J. Phys. Chem. B* **2005**, *109*, 8206.
(38) Hunter, C. A.; Sanders, J. K. M. *J. Am. Chem. Soc.* **1990**, *112*, 5525.
(39) Santos, P. S.; Amaral, J. H.; de Oliveira, L. F. C. *J. Mol. Struct.* **1991**, *243*, 223.
(40) Georgopoulos, S.; Diniz, R.; Rodrigues, B. L.; de Oliveira, L. F. C. *J. Mol. Struct.* **2005**, *741*, 61.
(41) Lee, K. S.; Seo, J. A.; Hwang, Y. H.; Kim, H. K.; Lee, C. E.; Nishiyama, K. *J. Korean Phys. Soc.* **2009**, *54*, 853.
(42) Rao, R.; Sakuntala, T.; Godwal, B. K. *Phys. Rev. B* **2002**, *65*, 054108.
(43) Kavitha, G.; Narayana, C. *J. Phys. Chem. B* **2007**, *111*, 7003.

(44) Hamann, S. D.; Linton, M. *Aust. J. Chem.* **1976**, *29*, 1825.
(45) Hamann, S. D. *Aust. J. Chem.* **1988**, *41*, 1935.
(46) Pravica, M.; Shen, Y.; Quine, Z.; Romano, E.; Hartnett, D. *J. Phys. Chem. B* **2007**, *111*, 4103.
(47) Katrusiak, A.; Szafrański, M. *J. Mol. Struct.* **1996**, *378*, 205.
(48) Mito, M.; Komorida, Y.; Tsuruda, H.; Tse, J. S.; Desgreniers, S.; Ohishi, Y.; Leitch, A. A.; Cvrkalj, K.; Robertson, C. M.; Oakley, R. T. *J. Am. Chem. Soc.* **2009**, *131*, 16012.